Anal Bioanal Chem (2009) 395:185–193
DOI 10.1007/s00216-009-2935-1

ORIGINAL PAPER

Engineered 3D tissue models for cell-laden microfluidic channels

Young S. Song · Richard L. Lin · Grace Montesano · Naside G. Durmus · Grace Lee · Seung-Schik Yoo · Emre Kayaalp · Edward Hæggström · Ali Khademhosseini · Utkan Demirci

Received: 21 June 2009 / Accepted: 23 June 2009 / Published online: 21 July 2009

Abstract Delivery of nutrients and oxygen within three-dimensional (3D) tissue constructs is important to maintain cell viability. We built 3D cell-laden hydrogels to validate a new tissue perfusion model that takes into account nutrition consumption. The model system was analyzed by simulating theoretical nutrient diffusion into cell-laden hydrogels. We carried out a parametric study considering different microchannel sizes and inter-channel separation in the hydrogel. We hypothesized that nutrient consumption needs to be taken into account when optimizing the perfusion channel size and separation. We validated the hypothesis by experiments. We fabricated circular microchannels (r= 400 μm) in 3D cell-laden hydrogel constructs (R= 7.5 mm, volume=5 ml). These channels were positioned either individually or in parallel within hydrogels to increase nutrient and oxygen transport as a way to improve cell viability. We quantified the spatial distribution of viable cells within 3D hydrogel scaffolds without channels and with single- and dual-perfusion microfluidic channels. We investigated quantitatively the cell viability as a function of radial distance from the channels using experimental data and mathematical modeling of diffusion profiles. Our simulations show that a large-channel radius as well as a large channel to channel distance diffuse nutrients farther through a 3D hydrogel. This is important since our results reveal that there is a close correlation between nutrient profiles and cell viability across the hydrogel.

Keywords 3D tissue engineering · Tissue perfusion · Microfluidic channel · Scaffold

Young Seok Song and Richard L. Lin have contributed equally to this contribution

Y. S. Song · R. L. Lin · G. Montesano · G. Lee · U. Demirci
Bio-Acoustic-MEMS in Medicine Lab,
HST Center for Bioengineering, Brigham and Women's Hospital,
Harvard Medical School,
65 Landsdowne Street #252,
Cambridge, MA 02139, USA

N. G. Durmus
Department of Biomedical Engineering, Boston University,
44 Cummington Street,
Boston, MA 02215, USA

S.-S. Yoo · A. Khademhosseini · U. Demirci
Brigham and Women's Hospital, Harvard Medical School,
Boston, MA 02115, USA

E. Kayaalp
Yeditepe University Faculty of Medicine,
26 Agustos Yerlesimi,
34755 Kayisdagi, Istanbul, Turkey

E. Hæggström
Electronics Research Laboratory, Department of Physics,
University of Helsinki,
POB 64, 00014, Finland

A. Khademhosseini · U. Demirci (✉)
Division of Health Sciences and Technology, Harvard-MIT,
Cambridge, MA 02139, USA
e-mail: udemirci@rics.bwh.harvard.edu

Introduction

Tissue-engineering technologies have important biomedical applications in areas such as organ transplantation and tissue regeneration [1, 2]. These technologies could benefit from synthetic tissues generated by culturing cells within vascularized three-dimensional (3D) extracellular matrix (ECM) scaffolds. These scaffolds serve as a synthetic ECM to organize seeded cells into a 3D architecture and to assist the growth and formation of tissues [3–6]. Ideally, a

scaffold should provide a nutrient-rich environment allowing cells to proliferate. It should also minimize cell death [7]. Several hydrogels (or hydrated polymer gels called aquagels) have been used as scaffolds for tissue engineering due to their mechanical and structural properties that mimic native tissue and ECM [6, 7].

Conventional scaffolding methods utilize cells cultured on two-dimensional (2D) substrates. Native tissue, on the other hand, comprises complex 3D cell-matrices, which limits the predictive power of the results obtained with these 2D methods [8–10]. Cells seeded within diffusively permeable constructs need 3D mechanical support as well as nutrient and soluble factor delivery. Moreover, cells in these constructs experience an environment that mimics in vivo conditions [11]. Such constructs should also be composed of materials, e.g., hydrogels that allow cell seeding to feature mass-transfer characteristics adequate for nutrient/soluble factor exchange. Agarose hydrogels provide attractive properties including moldability, high porosity, and diffusion control [12–17]. They can be used in cartilage and vascular tissue engineering since they exhibit high diffusivity to oxygen and other water-soluble metabolites [12, 14]. Engineering hydrogel tissue scaffolds can enhance this perfusion capacity that is necessary to maintain high cell viability [18–21]. Therefore, one needs to characterize the tissue scaffolds through experiments and theoretical simulations to achieve high cell viability.

Microfluidics is a powerful tool for biological analysis [22–25]. Microfluidic channels are engineered to facilitate nutrient and soluble factor exchange within synthetic cell-laden hydrogel constructs [4]. Microfluidic channels formed within the cell-embedded agarose were used to simulate basic circulatory functions, such as providing nutrients to the cells [26–28]. The channels are also potentially suitable to promote vascularization [18, 29]. There is a need to examine the nutrient and soluble factor distributions in cell-laden hydrogel structures featuring microfluidic channels since the cell viability is strongly correlated with the nutrient distribution within these constructs. This can be done by developing a 1D diffusion model as a control using cell-laden agarose constructs without channels in a Petri dish. This step can then be followed by developing a 2D perfusion model in which cell medium is flowed through single and dual fluidic channels in hydrogel constructs. In addition, nutrient-diffusion profiles as a function of distance from the source can be theoretically simulated for these three architectures. These theoretical results can then be used to determine optimal dimensions of those models and to understand the experimental viability results. Overall, this approach could offer a direction towards synthetic vascularized tissue engineering by presenting an analytical link between nutrient distribution and viability in 3D hydrogel constructs.

Theoretical modeling

We consider the following assumptions [30]: (1) agarose hydrogel has high porosity, permeability, and diffusivity, (2) the cell viability in the hydrogel structure depends on the diffusion of nutrients, (3) cells in the hydrogel consume nutrients and are proliferated, and (4) the diffusion behavior of the hydrogel structure can be modeled macroscopically by using the concept of a representative elementary volume (REV), i.e., repeating unit volume [31]. From a microscopic point of view, nutrients and soluble factors are described in an unobstructed medium using the following equation:

$$\frac{\partial c}{\partial t} = D\nabla^2 c + s \tag{1}$$

where c is the concentration of nutrients, D is the diffusion coefficient, and s is the source or sink density. Here, s acts as a sink because cells in the hydrogel consume nutrients and soluble factors over time. The concentration profiles of the nutrients are discontinuous across the hydrogels since cell-laden hydrogels encompass intracellular and extracellular phases. As a result, it is convenient to employ the spatially averaged concentration with respect to REV to macroscopically analyze the diffusion of nutrients in the hydrogel [31]:

$$\langle c \rangle = \frac{1}{V}\int_{V_0} c dV \tag{2}$$

in which V is the representative elementary volume (REV) and V_0 is the volume of the extracellular phase where diffusion takes places. By invoking the average concept of Eq. 2, Eq. 1 can be rewritten as

$$\frac{\partial < c_0 >}{\partial t} = D^* \nabla^2 < c_0 > + \frac{< s >}{\alpha} \tag{3}$$

where c_0 is the concentration in the extracellular space, α is the volume fraction of the extracellular space defined as $\frac{V_0}{V}$, and $D^* = \frac{D}{\lambda^2}$ (λ is the tortuosity of the hydrogel). After further justification [31], Eq. 3 can be expressed as:

$$\frac{\partial c}{\partial t} = D^*\nabla^2 c + \frac{s}{\alpha} \tag{4}$$

The above partial differential equation, which is analogous to the classical diffusion Eq. (1), is solved using an iterative solver based on the finite element method (FEM). The physico-chemical properties of Eq. (4) are obtained from the literature [31, 32].

Materials and methods

To validate the new model, we carried out experiments. First, we investigated the 1D nutrient-diffusion behavior in a Petri dish setup without channels (Fig. 1a). Then, we

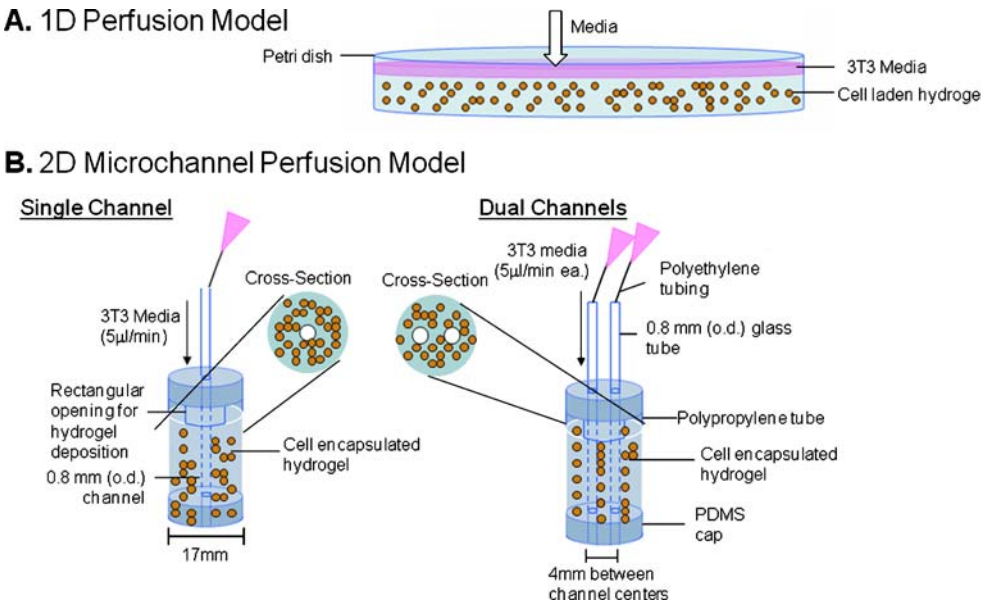

Fig. 1 Schematic of our perfusion studies. **a** 1D perfusion/viability model: cell-laden hydrogel was prepared in a Petri dish. The cells were then perfused by the cell media poured on top of the hydrogel. **b** 2D microchannel perfusion/viability model: single- and dual-channeled hydrogel constructs were prepared using cell-laden agarose

established the 2D perfusion system by fabricating hydrogel constructs around 0.4-mm glass capillary tubes that allow forming a watertight agarose scaffold with one or two adjacent circular microfluidic channels. The research methodology presented in Fig. 1 is explained in detail below.

Single- and dual-channel devices were constructed as follows. Cells suspended in molten agarose with a low gelling temperature (30°C) were molded into microfluidic channels. The cells remain viable and are evenly mixed within the scaffold during construction [12, 29, 33]. Culture medium was pumped through straight tubular channels to facilitate nutrient transfer to the embedded cells. Cell viability was examined for at least 3 days to allow the benefits due to a multiple channel design to be observed [12].

Cell cultures

NIH-3T3 murine embryonic fibroblasts (CRL-1658, ATCC, Manassas, Virginia) were kept at 37ºC in a sterile 5% CO_2 95% air incubator (Model 3110, Forma Scientific, Marietta, Ohio). The cells were cultured in 3T3 medium composed of 90% Dulbecco's Modified Eagle Media (DMEM, Gibco), 9% Fetal Bovine Serum (FBS, Gibco), and 1% penicillin–streptomycin (Sigma Aldrich St. Louis, MO). Once confluent, the 25-cc flasks were passaged (subculture ratio 1:4 for multiple flasks) every 3–4 days for both experiments.

1D perfusion model in a Petri dish

Liquid agarose and 3T3 cells were pipetted and mixed to obtain a uniform (5×10^5 cells/ml) agarose-cell mixture. The cells were evenly distributed in the hydrogel after gelling. The liquid mixture was poured into a Petri dish and covered with 3T3 medium (Fig. 1a). The Petri dish containing the cell-laden agarose was kept in an incubator at 37ºC with 5% CO_2 between the daily assessments. Thus, the cell viability profile in this classic 2D setup (1D perfusion model) was determined. The viability profile provides a baseline and acts as a control for the perfusion distance and cell viability in agarose.

2D perfusion model in hydrogel constructs

Agarose hydrogels were generated using agarose in 1× phosphate-buffered saline (PBS, Gibco, Invitrogen, Carlsbad, California). Three grams of agarose was dissolved and heated (700 W, 30 s) in a microwave oven (Model M0902SST-1, Avanti, Miami, FL) in 100 ml PBS. After first trypsinizing the confluent cells in flasks, we resuspended and centrifuged them (Beckmann Coulter, Fullerton, CA) at 1,000 rpm for 5 min. Then, the cell pellets were introduced into agarose that was cooled from ~55ºC and pipetted to ensure even cell distribution (5×10^5 cells/ml) before the agarose solidified at ~30ºC.

Single-channel tubular microfluidic channels were constructed within the cell-laden agarose as the hydrogel solidified (3% agarose, Low Gelling Temperature Type VII, Sigma Aldrich, St. Louis, Missouri) inside clear 17-mm diameter polypropylene tubes (Becton Dickinson, Franklin Lakes, NJ; Fig. 1b). Fabrication was done in a sterile hood. A rectangular opening was cut near the end of the tube to provide an opening to deposit the cell-laden agarose mixture. Polydimethylsiloxane (PDMS; Sylgard® 184 Silicone Elastomer Kit, Dow Corning, Midland, Missouri) was used to mold caps to fit the two open ends of the plastic tubes. Once the caps were fabricated, 300-µm-diameter canals were drilled through the caps. Then, 300-µm-diameter glass

capillary tubes (Charles Supper Company, Natick, Massachusetts) were threaded through the PDMS cap into polypropylene tubes (Small Parts, Inc., Miami Lakes, Florida). The opposite ends of each tube were sealed to polyethylene tubing (8.89 mm outer diameter, Small Parts, Inc., Miami Lakes, Florida) with PDMS. This tubing was then attached to a needle with Luer hubs (NE-301PL-C, Small Parts, Inc., Miami Lakes, Florida), again with PDMS. The glass capillary tube of this contraption was weaved through the hole in the top cap of the plastic tube. Parafilm Laboratory Film (Pechiney Plastic Packaging, Chicago, Illinois) was used to tightly seal the bottom end of the tubes (Fig. 1b).

After this step, 5 ml of molten, cell-laden agarose was poured through the rectangular device opening and left to solidify around the glass capillary tube for 1 h. Once fully gelled, the parafilm piece was removed. The glass capillary tubes were withdrawn slightly and the bottom PDMS caps were removed and replaced with another PDMS cap featuring a square opening to allow unobstructed access to the agarose. Once this step was completed, the glass capillary tubes were further withdrawn, leaving 1 cm of the glass tube within the agarose gel. The Luer hubs were then attached to 10-ml syringes (Becton Dickinson) filled with cell medium. The plastic tubes containing the molded agarose were placed upright in Styrofoam test tube racks. The tube preparation method is the same for the two-channel experiments except that the caps have two holes that are 4 mm apart instead of a single hole in the center for the dual-channel experiments (Fig. 1b).

Channel fabrication and molding

The cell-laden agarose construct featured a tubular channel within a plastic tube. A low agarose concentration affected the mechanical properties of the scaffold construct. A low (<3%) agarose concentration produced a structurally weak agarose that collapsed under the combined channel weight and fluidic pressure. A high agarose concentration (> 6%) was difficult to handle, as the agarose gelled rapidly after cell seeding. After testing, 3% agarose concentration was found suitable for channel fabrication. This concentration produced a firm, semi-translucent agarose material that withstood the channel weight and fluidic pressure.

Channel flow rate

After the microfluidic channel was constructed, 3T3 nutrient medium was pumped through it for 3 days. The flow rate was controlled by a multiple syringe pump (AL-8000, World Precision Instruments, Sarasota, FL). Syringes loaded with 3T3 medium were attached to the syringe pump. The emanating 3T3 medium deposit was collected using a Petri dish placed under the styrofoam test tube racks.

Cell nutrient medium was pumped through the constructed tubular channels to transfer nutrients to the embedded cells. For both the single-channel- and the two-channel experiments, the 3T3 medium was pumped at a rate of 5 μl/min. Sterile conditions were maintained by constructing and fabricating the device and microfluidic channel within a fume hood and by keeping the entire device setup running in a 5% CO_2 sterile incubator at 37 °C. After perfusion, the 3D construct was cut into three disks to verify an even cell distribution within the construct and to verify the viability at multiple locations. The agarose-encapsulated cells were distributed evenly, as qualitatively verified by visual inspection under a microscope, within the scaffold.

Analytical and quantitative techniques

Cell viability within the microfluidic channels was examined by applying a live/dead fluorescence assay (Molecular Probes, Invitrogen, Carlsbad, California) to the slices of agarose containing embedded cells. The orientation and dimensions of the analyzed hydrogel sections are defined in Fig. 5a. The circular rings of live/dead cells were counted from the center and obtained as a function of spatial location. Due to the circular symmetry of the single-channel hydrogels, we counted cells on one half-side of the slice to determine the cell viability. For the dual-channel hydrogels, we identified and counted the live and dead cells on both sides to obtain the cell viability after 1, 2, and 3 days. Specifically, the PDMS end caps were removed and the molded agarose was allowed to slip out of the plastic tube. Front, middle, and end disks of agarose, each 1 mm thick, were carefully cut with a razor blade. The slices were immersed into the live/dead assay reagent immediately after slicing to obtain accurate cell counts, Fig. 5. The cut was made orthogonal to the agarose cylinder symmetry axis. The top surface was defined as the one facing upstream with respect to the flow direction. The top surface of the middle disk was 25 mm from the top of the agarose droplet structure in the pipette tip. Live/dead stain was prepared by brief mixing (multiple consecutive pipetting) of 0.5 μl calcein AM (Molecular Probe, Invitrogen) and 2 μl ethidium homodimer-1 (Molecular Probe, Invitrogen) per 1 ml of 1× PBS solution (Gibco 14100, Invitrogen, Carlsbad, California). The agarose disks were submerged into the live/dead stain solution and incubated for 10 min at 37 °C. Then the live/dead stain was aspirated off, and the disks were examined at 40× magnification using an inverted fluorescent microscope (Nikon, TE2000, Enfield, CT). Each agarose disk was imaged starting from the center of the channel and extending radially outward. Sections of the molded agarose tube were imaged to ensure that the cells were uniformly distributed along the channel. Live

and dead cells were identified by the emission of green and red fluorophores, respectively. As seen in Fig. 5a, the fraction of living cells was determined by counting the number of live (green) cells versus the number of dead (red) cells (Image J program, National Institutes of Health, Bethesda, Maryland) under 40× magnification and by dividing the number of the live cells by the number of total cells (live plus dead).

Results and discussion

Numerical modeling of nutrient distributions

The viability of cells embedded in a hydrogel is determined by how nutrients and soluble factors diffuse through the cell-laden hydrogels. Understanding the transport behavior of nutrients in the hydrogel allows us to interpret the cell viability results. In the current study, the nutrient distributions in the cell-laden hydrogel were predicted by simulations. To evaluate the effect of the geometry and dimension of perfusion models, we performed a parametric study, where we changed the microchannel diameter and inter-channel distance. Figure 2a and b present the diffusion behavior of nutrients for the 2D-perfusion model with a single channel and dual channels, respectively. The nutrient concentration is normalized by using the nutrient concentration at the surface of the cell culture media source. As the channel radius increases, nutrients can diffuse further away from the channels through the hydrogels. For instance, in the case of r=0.2 mm, a depletion zone with no nutrients is found from 5 mm outward from the channel (Fig. 2b). Such a zone, however, disappears with increasing microchannel size. On the other hand, due to the existence of an optimal ratio of the perfusion channel volume to the total construct volume, there is a limitation to increasing the size of channels in the hydrogel. One should note that there is a tradeoff between the total cell-laden hydrogel volume and the channel volume. We fixed the channel radius at 0.4 mm and considered different inter-channel distances in the calculation (Fig. 2c). As the inter-channel distance is increased, the effect of inter-channel diffusion of nutrients on the total nutrient diffusion becomes significant.

For a 0.4-mm radius and 4 mm inter-channel distance for the 2D perfusion model, the distribution contours of nutrients across the hydrogel are presented in Fig. 3a–c. Figure 3c shows that the nutrients of the 2D perfusion model with dual channels diffuse further away from the media source than those of the 2D perfusion model with a single channel (Fig. 3b). This result explains why the dual-channel perfusion model is more efficient in transferring nutrients to cells embedded in the hydrogel structure. Consequently, the dual channel structure can provide higher

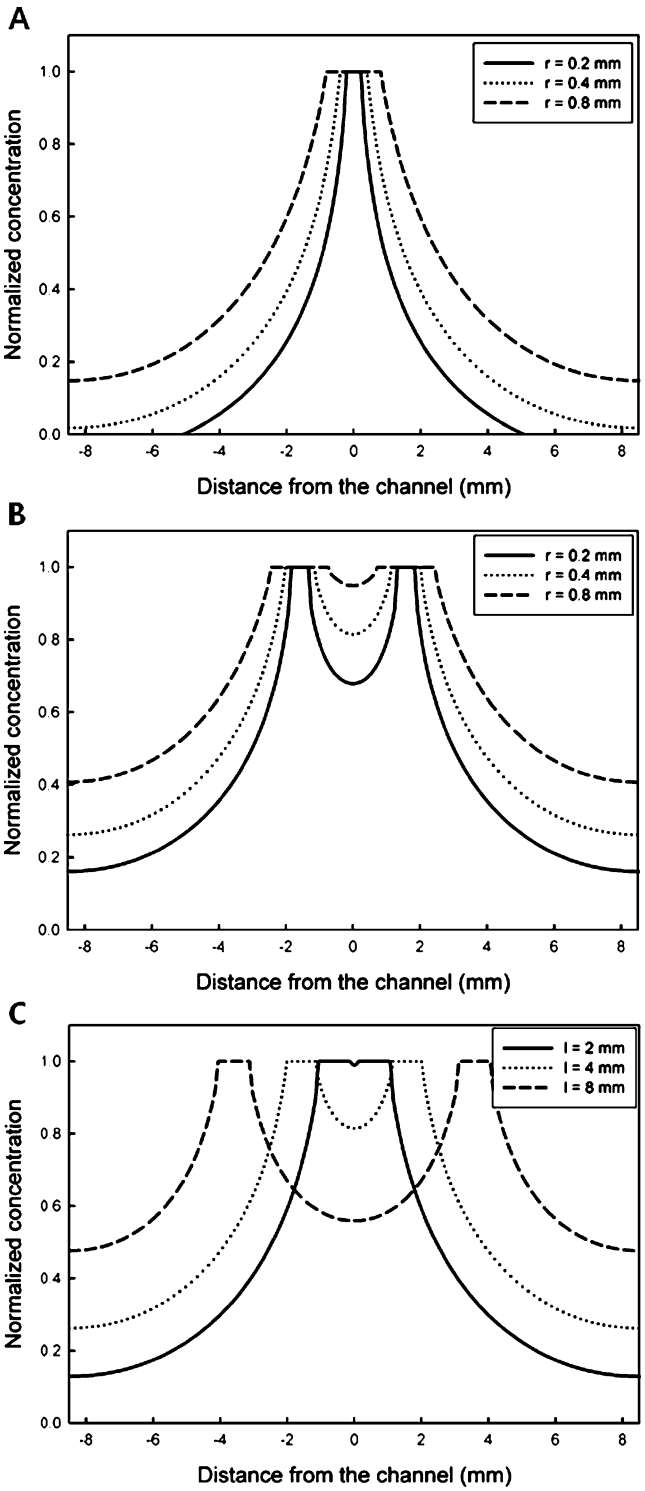

Fig. 2 Numerical simulation of the effect of different radii and interdistances of channels. **a** Nutrient distribution for the 2D perfusion model with a single channel at day 1. **b** Plot of the normalized concentration for the 2D perfusion model with dual channels as a function of distance from the channel. **c** Concentration profiles of nutrients for the 2D perfusion model with dual channels with respect to distance from the channel

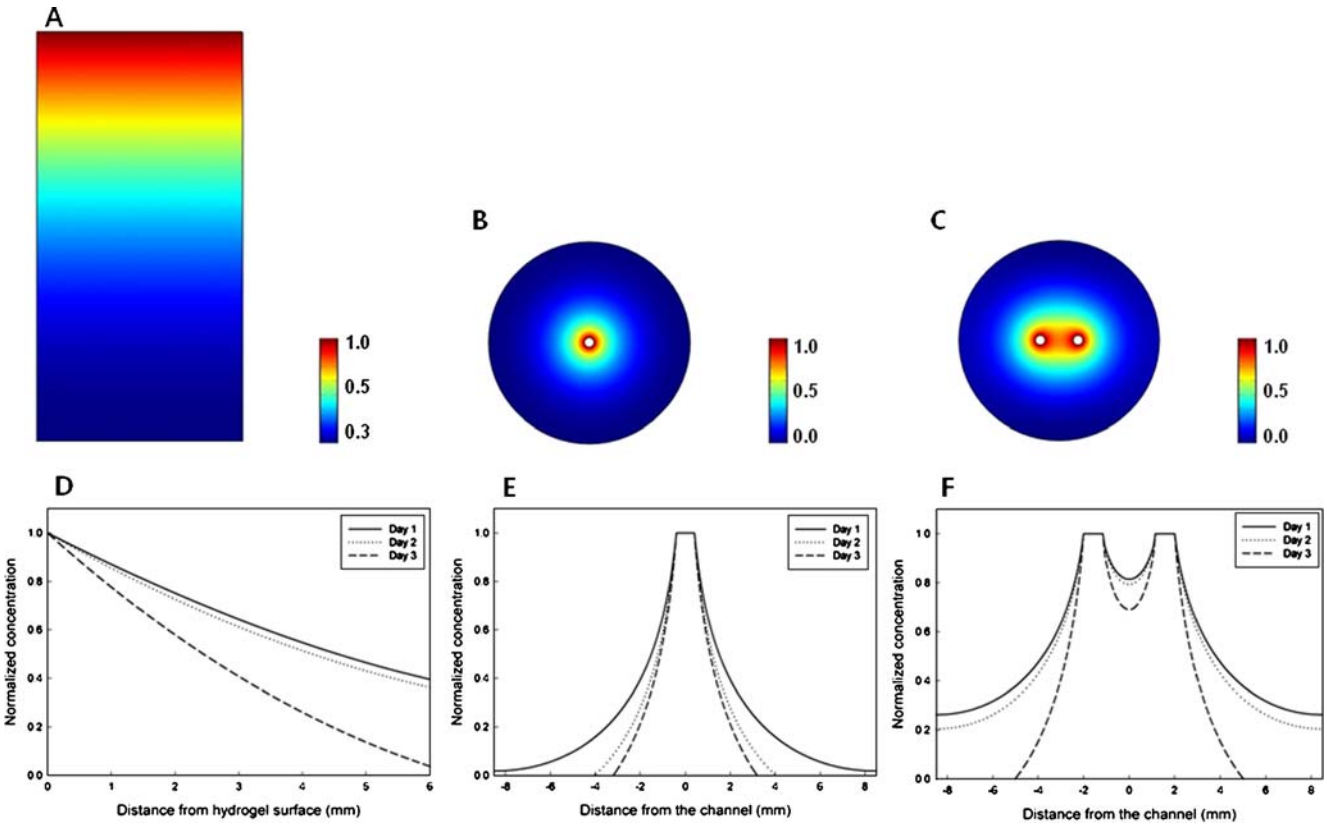

Fig. 3 Theoretical analyses of nutrition diffusion in an agarose hydrogel. **a** Distribution of nutrients for the 1D perfusion model at day 1. **b** Contour of the nutrition concentration for the 2D perfusion model with a single channel at day 1. **c** Distribution of nutrients for the 2D perfusion model with dual channels at day 1. **d** Plot of the normalized concentration of nutrients for the 1D perfusion model as a function of distance from the hydrogel surface. The nutrient concentration decreases with increasing distance. **e** Nutrient concentration for the 2D perfusion model with a single channel as a function of distance from the channel. **f** Plot of the normalized concentration of nutrients for the 2D perfusion model with dual channels as a function of distance from the channel

cell viability across the hydrogel than the 2D perfusion model with a single channel. It is assumed that live cells in the hydrogel consume nutrients and soluble factors. Once cells near the media source have consumed most of the nutrients, the rest of cells in the hydrogel cannot get sufficient nutrients, thereby facing cell death. Figure 3d–f present the change in the nutrient concentration as a function of the distance from the hydrogel or channel surface. Since the cells near the channel surface consumed nutrition, the distribution of nutrients grew steeper across the hydrogel over days. This is distinct from a common diffusion profile, which tends to approach a flat uniform concentration. In comparison to Fig. 3e, f illustrates the higher normalized concentration. That is, at day 3, the depletion zone of the 2D perfusion model with a single channel is found to be from 3.2 to 7.5 mm (or −3.2 to −7.5 mm), while that of the 2D perfusion model with dual channels is 5 to 7.5 mm (or −5 to −7.5 mm). We assume that cells in the depletion zone were provided with sufficient nutrients. Consequently, the 2D perfusion model with dual channels predicts that we can have higher cell viability due to a more uniform nutrient diffusion by employing this construct.

1D perfusion/viability model in a Petri dish setup

To validate the simulation predictions we carried out a set of experiments. We determined during a 3-day time period the 1D viability profile of NIH-3T3 cells residing in agarose. The absolute initial cell viability in the Petri dish after seeding was 89% on average. As predicted, the cell viability significantly decreased both with increasing distance from the nutrient source and as a function of time elapsed after cell seeding. We recorded cell viability, relative to the initial control taken after cell seeding, in a 45-mm radius and 50-mm-thick agarose disk (Fig. 4a). We found the projected cell viability to be comparable to literature values of approximately 60% viability for day 3 [12, 34–36]. We observed that fibroblast (NIH-3T3) cell viability was maximized close to the surface, and that it exceeded 60% within 5-mm radial distance from the channel on day 3 (Fig. 4b).

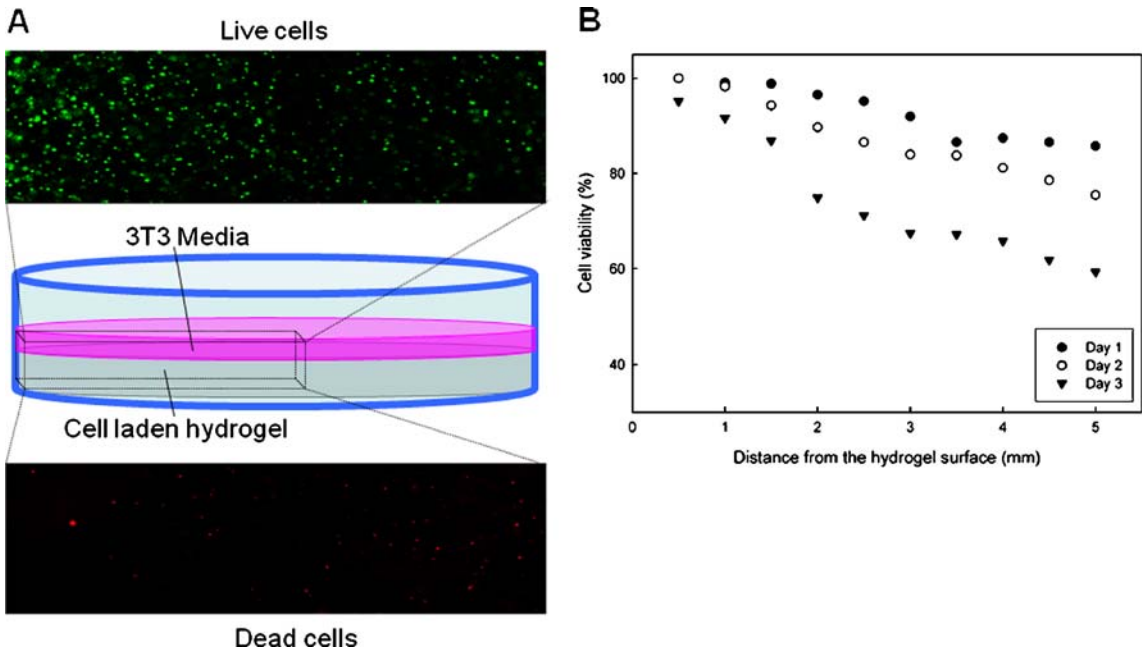

Fig. 4 1D perfusion model. **a** The diagram summarizes the initial 1D perfusion experiment setup. Cell-laden hydrogel was poured into a 10-cm diameter Petri dish and left to gel. Live/dead fluorescent images obtained from one cross section of cell-laden agarose. Live 3T3 cells are green and dead cells are red. **b** A plot of fractional viability (absolute number of live cells versus dead cells) taken at 500-μm increments from the surface of the Petri dish over 1, 2, and 3 days

2D perfusion/viability model with microchannels

We fabricated single and dual-microfluidic channels in agarose without relying on soft lithography. These channels featured a circular cross section to yield a cylindrical cell viability pattern (Fig. 5a).

For single-channel constructs, the cell viability data were presented in Fig. 5b–d (89% average cell viability). The cell viability decreased both with increasing distance from the *single* channel and as a function of time elapsed after cell seeding. We recorded the relative cell viability in a 7.5-mm radius and 50-mm-long agarose cylinder (15 data points) and plotted the viability data against time (Fig. 5b–d). This compares favorably with the literature values of ~50% viability at day 3.[12, 34–36] We observed that the relative NIH-3T3 cell viability was maximized close to the microfluidic channels (98.4±1.37%) exceeding 90% at approximately 3 mm radial distance for day 1. On the other hand, we found that the nutrient depletion across the hydrogel is a function of distance from the channel. The experimental viability data follow the same trend as the theoretical profiles in Fig. 3.

The cell viability of the dual-channel model decreased both with increasing distance from the *dual* channels and as a function of time elapsed after seeding. However, the decrease in viability was found much less than that of the single-channel model as shown in Fig. 5b–d. Using dual channels, we demonstrated broader diffusion profiles than what is possible with a single-channel in a 3D tissue construct. Subsequently, when compared to the single-channel case, the dual-channel construct provided significantly broader viability profiles. This improved the total cell viability by at least 20% especially later into the experiment (day 3). Specifically, for day 1, the lowest viability percentage for dual channels along the near perimeter of the cylindrical agarose construct was 90%, while for a single channel it was 64%. For day 2, the dual-channel construct showed 85% cell viability (again near the outside perimeter), while the single-channel construct achieved 60%. For day 3 experiments, the relative cell viability remained at 80% for dual channels, while for a single channel the relative cell viability dropped to 50%. These experimental results show that dual channels improve cell viability within the construct as predicted by the theoretical simulations. In other words, since the dual channel model can achieve narrower depletion zones of nutrients across the hydrogel over time than the single channel model (Fig. 3e and f), the cell viability measured in the dual channel model exceeded that in the single channel.

In summary, we investigated 3D tissue engineering approaches to combine microfluidic channels directly merged with agarose. We prepared perfusion models with cell-laden hydrogels based on simulations of nutrient diffusion in the hydrogels and characterized the corresponding cell viability experimentally. The study

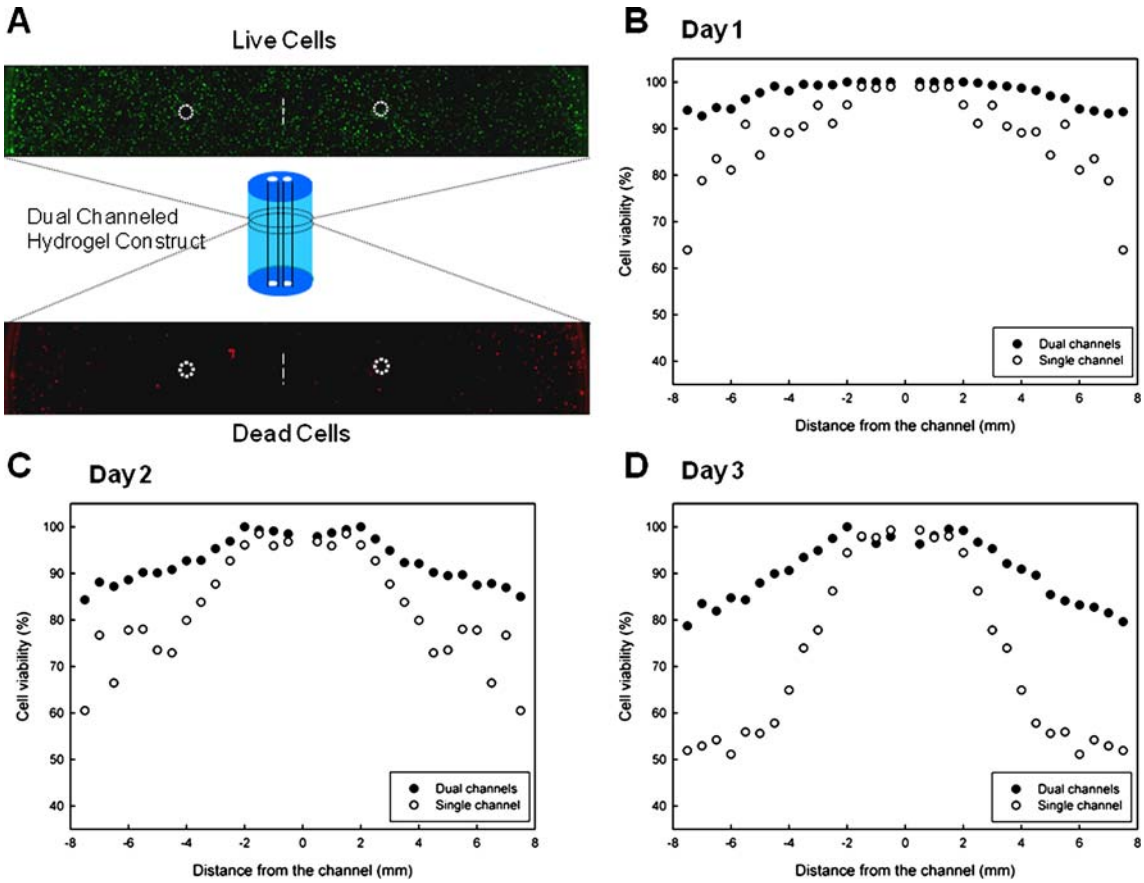

Fig. 5 2D microchannel perfusion model. **a** Schematic drawing of a dual parallel microchannel device. Top view of radial slab where channels and symmetry center are indicated. Live/dead fluorescent images obtained 48 h into the experiment from slices of cell-laden agarose with a radial viability setup and two microchannels. The *circled regions* mark the location of the channels. **b**, **c**, **d** Plots of fractional cell viability with single- and dual-channel setups taken at day 1, 2, and 3, respectively, after the channel constructs were built. We counted the live and dead cells on both sides of dual-channel hydrogels. The reference level is the viability control of 89% viability from day 0

provided experimental and theoretical understanding about nutrient perfusion and cell viability in 3D cell-laden agarose constructs. These approaches could help to engineer 3D complex tissue constructs of optimized dimensions. They could also potentially be applied to constructs built using other cell types such as cancer and stem cells maintaining viability for extended time periods. In addition our approach could enable creating 3D tissue constructs to mimic native tissues in vitro.

Conclusion

We studied perfusion in a microfluidic, 3D cell-laden hydrogel construct for tissue engineering applications. We fabricated microscale channels (r=0.4 mm) with circular cross section in agarose constructs (r=7.5 mm, volume= 5 ml). These channels were positioned in parallel in close proximity to improve perfusion in the cell-laden hydrogels. We numerically analyzed spatial and temporal transport behavior of nutrients for the perfusion models prepared in the current study. We also investigated the effect of channel size and inter-channel separation on the diffusion distribution of nutrition across the hydrogel. From our simulations, we found that larger radius channels and larger inter-channel separation lead to further diffusion of nutrients through the hydrogel. The results revealed that nutrients could not diffuse far away from the media source due to the nutrient consumption. Also, the resulting cell viability decreases with an increase in distance from the media source. These findings also confirm that there is a close correlation between nutrient profiles across the hydrogels and cell viability. On the other hand, the 2D perfusion model with dual channels was found to provide improved cell viability compared to that of a single channel. These scaffold-based approaches to control the cell microenvironment could enhance our understanding to perfuse and engineer 3D complex tissue constructs.

Acknowledgment We would like to thank the Randolph Hearst Foundation and Department of Medicine, Brigham and Women's Hospital for the Young Investigators in Medicine Award. This research is performed at the Bio-Acoustic-MEMS in Medicine (BAMM) Labs, HST Center for Bioengineering, Brigham and Women's Hospital, Harvard Medical School.

Author contributions YSS, RLL, UD, and EH wrote the paper. YSS carried out the simulation. GM and GL performed the experiments and collected data. YSS created the model and the theoretical analysis. RLL, YSS, GM, EH, and UD conducted the data analyses. GD, SSY, EK, AK, and EH read and gave feedback on the paper.

References

1. Khademhosseini A, Langer R, Borenstein J, Vacanti JP (2006) Proc Natl Acad Sci 103:2480–2487
2. Orive G, Hernández RM, Gascón AR, Calafiore R, Chang TMS, De Vos P, Hortelano G, Hunkeler D, Lacík I, James Shapiro AM, Pedraz JL (2003) Nat Med 9:104–107
3. Drury JL, Mooney DJ (2003) Biomaterials 24:4337–4351
4. Hollister SJ (2005) Nat Mater 4:518–525
5. Yang S, Leong K, Du Z, Chua C (2001) Tissue Eng 7:679–689
6. Choi NW, Cabodi M, Held B, Gleghorn JP, Bonassar LJ, Strook AD (2007) Nat Mater 6:908–915
7. Baksh D, Davies JE (2000) Design strategies for 3-dimensional in vitro bone growth in tissue-engineering scaffolds. University of Toronto Press, Toronto
8. Kim J (2005) Semin Cancer Biol 15:365–377
9. Pickl M, Ries CH (2009) Oncogene 28:461–468
10. Abbott A (2003) Nature 424:870–872
11. Khademhosseini A, Eng G, Yeh J, Kucharczyk P, Langer R, Vunjak-Novakovic G, Radisic M (2007) Biomed Microdevices 9:149–157
12. Ling Y, Rubin J, Deng Y, Huang C, Demirci U, Karp JM, Khademhosseini A (2007) Lab Chip 7:756–762
13. Khademhosseini A, Eng G, Yeh J, Fukuda J, Blumling J, Langer R, Burdick JA (2006) J Biomed Mater Res Part A 79:522–532
14. Nedović V, Willaert R(2003) Fundamentals of Cell Immobilisation Biotechnology, Kluwer, New York
15. Peter Lundberg PWK (1997) Magn Reson Med 37:44–52
16. Rotem A, Toner M, Bhatia S, Foy BD, Tompkins RG, Yarmush ML (2004) Biotechnol Bioeng 43:654–660
17. Augst AD, Kong HJ (2006) Mooney DJ 6:623–633
18. Xu T, Gregory C, Molnar P, Cui C, Jalota S, Bhaduri SB, Boland T (2006) Biomaterials 27:3580–3588
19. Mittal SK, Aggarwal N, Sailaja G, van Olphen A, HogenEsch H, North A et al (2000) Vaccine 19:253–263
20. Stevens MM, Qanadilo HF, Langer R (2004) Biomaterials 25:887–894
21. Zimmermann H, Reuss R, Feilen PJ, Manz B, Katsen A, Weber M, Ihmig FR, Gessner P, Behringer M, Steinbach A, Wegner LH, Sukhorukov VL, Schneider S, Weber MM, Volke F, Wolf R, Zimmermann U (2005) J Mater Sci Mater Med 16:491–501
22. Weibel DB, Whitesides GM (2006) Curr Opin Chem Biol 10:584–591
23. Nguyen KT, West JL (2002) Biomaterials 23:4307–4314
24. Albrecht DR, Tsang VL, Sah RL, Bhatia SN (2005) Lab Chip 5:111–118
25. Demirci U, Montesano G (2007) Lab Chip 7:1139–1145
26. Khademhosseini A, May MH, Sefton MV (2005) Tissue Eng 11:1797–1806
27. Chrobak KM, Potter DR, Tien J (2006) Microvasc Res 71:185–196
28. Nahmias Y, Kramvis I, Barbe L, Casali M, Berthiaume F, Yarmush ML (2006) FASEB J 20:E1828–E1836
29. Shin M, Matsuda K, Ishii O, Terai H, Kaazempur-Mofrad M, Borenstein J et al (2004) Biomed Microdevices 4:269–278
30. Fatin-Rouge N, Starchev K, Buffle J (2004) Biophys J 86:2710–2719
31. Nicholson C (2001) Rep Prog Phys 64:815–884
32. Frykman S, Srienc F (1998) Biotechnol Bioeng 59:214–226
33. Jones KS, Sefton MV, Gorczynski RM (2004) Transplantation 78:1454–1462
34. Gehrke SH, Fisher JP, Palasis M, Lund ME (1997) Ann N Y Acad Sci 831:179–207
35. Khademhosseini A, Yeh J, Jon SY, Eng G, Suh KY, Burdick J, Langer R (2004) Lab Chip 4:425–430
36. Volokh KY (2006) Acta Biomater 2:493–504